Available online at www.sciencedirect.com
ScienceDirect
Trans. Nonferrous Met. Soc. China 32(2022) 3301−3311
Transactions of Nonferrous Metals Society of China
www.tnmsc.cn

Combined effects of Bi and Sb elements on microstructure, thermal and mechanical properties of Sn−0.7Ag−0.5Cu solder alloys

Suchart CHANTARAMANEE[1], Phairote SUNGKHAPHAITOON[2]

1. Department of Industrial Engineering, Faculty of Engineering,
Rajamangala Unversity of Technology Srivijaya, 90000 Songkhla, Thailand;
2. Division of Physical Science, Faculty of Science, Prince of Songkla University, Hat Yai, 90110 Songkhla, Thailand

Received 11 August 2021; accepted 27 December 2021

Abstract: This research investigated the combined effects of addition of Bi and Sb elements on the microstructure, thermal properties, ultimate tensile strength, ductility, and hardness of Sn−0.7Ag−0.5Cu (SAC0705) solder alloys. The results indicated that the addition of Bi and Sb significantly reduced the undercooling of solders, refined the β-Sn phase and extended the eutectic areas of the solders. Moreover, the formation of SbSn and Bi phases in the solder matrix affected the mechanical properties of the solder. With the addition of 3 wt.% Bi and 3 wt.% Sb, the ultimate tensile strength and hardness of the SAC0705 base alloy increased from 31.26 MPa and 15.07 HV to 63.15 MPa and 23.68 HV, respectively. Ductility decreased due to grain boundary strengthening, solid solution strengthening, and precipitation strengthening effects, and the change in the fracture mechanism of the solder alloys.

Key words: Sn−0.7Ag−0.5Cu solder alloys; intermetallic compounds; strengthening mechanism; undercooling; mechanical properties

1 Introduction

Solder alloy is an important material in the electronics industry. It is used to connect electronic components to circuit boards. In the past, tin−lead (Sn−Pb) solder was commonly used in electronic devices since it had good soldering properties and was cheap cost [1]. However, lead was banned as an ingredient in solders due to its toxic effects on human health and environmental contamination. Therefore, Sn−Pb solders have been replaced with new lead-free solders that still use tin as the main component. Solder alloys such as Sn−Cu [2,3], Sn−Ag [4,5], Sn−Bi [6−8], Sn−Sb [9,10], Sn−Zn [11,12], and Sn−Ag−Cu [13,14] have been developed. Electronics industries, especially, use lead-free solders containing tin (Sn), silver (Ag), and copper (Cu) for their near-eutectic compositions, high strength, good solderability, and high fatigue resistance [15,16]. However, solders in the Sn−Ag−Cu (SAC) alloy group have some drawbacks that need to be overcome. SAC solders have higher melting points than Sn−Pb solders, the formation of coarse Ag_3Sn IMC phases can weaken solder joints, and the growth of IMC layers along the interface during soldering reduces solder joint reliability [17,18]. To overcome these limitations, some properties of SAC solders have to be improved.

The melting point of SAC solders has been reduced by adding elements such as indium (In), gallium (Ga), and bismuth (Bi) [19−24]. Their microstructures have been refined and mechanical properties have been enhanced with the addition of elements such as zirconium (Zr) [17], Bi [21−24],

Corresponding author: Phairote SUNGKHAPHAITOON, E-mail: phairote.s@psu.ac.th
DOI: 10.1016/S1003-6326(22)66021-7

antimony (Sb) [25−28], zinc (Zn) [29,30], titanium (Ti) [31], aluminium (Al) [32,33], cobalt (Co) [34], and rare earth elements (RE) [35,36]. A review of previous research found that the addition of Bi to SAC solder alloy groups exhibited refined β-Sn dendrite microstructures, fine Bi precipitates in the β-Sn matrix, improved wettability, reduced melting points and undercooling, increased yield strength, tensile strength, and hardness of the solder alloy due to fine precipitate dispersion strengthening and solid solution strengthening mechanisms. Moreover, Bi suppressed the growth of Cu_3Sn and Cu_6Sn_5 IMC in the interfacial layer and increased shear strength of the solder joint [21−24]. Elsewhere, a small addition of Sb to SAC solder slightly increased melting point, reduced undercooling, refined the dendritic size of β-Sn, enhanced tensile strength and improved creep properties due to the strengthening effect of the SnSb solid solution. Besides, Sb inhibited the growth of IMC interfacial layers and reduced the thickness of the interface of the solder joint. As a result, the shear strength of the solder joint was increased [25−27]. In addition, large amounts of Sb (25−31 wt.%) added to SAC solder alloy formed new $Ag_3(Sn,Sb)$ IMCs and a large SbSn phase in the β-Sn matrix. Larger addition of Sb significantly increased the melting temperature of the solder alloy. Ultimate tensile strength also increased with increments of Sb but elongation decreased due to the solid solution hardening effect of Sb [28].

A review of the literature [21−27] confirmed that the addition of Bi and Sb elements can refine β-Sn phases and eutectic structures, and enhance mechanical properties of Sn−Ag−Cu solder alloys. Therefore, this research presented a study of the combined effects of Bi and Sb elements on the microstructure, melting point, hardness, tensile strength, and ductility of SAC0705 solder alloys.

2 Experimental

2.1 Solder specimen preparation

The solder alloys used in the following experiments were Sn−0.7Ag−0.5Cu−xBi−xSb systems, where x=0, 1, 2, and 3 wt.%. The solder specimens were respectively referred as SAC-0705, SAC0705−1Bi−1Sb, SAC0705−2Bi−2Sb, and SAC0705−3Bi−3Sb and their compositions are listed in Table 1. High purity Sn (99.95%), Cu (99.99%), Ag (99.99%), Bi (99.95%), and Sb (99.95%) ingots were used to prepare the alloys. Initially, a graphite crucible was charged with metal ingots and heated in an electric furnace at 400 °C for 6 h. The molten alloy was allowed to cool to 270 °C to prevent high-temperature oxidation and then agitated with a mechanical stirrer for 10 min to homogenize the melt. Before casting, the steel mold was preheated to 200 °C to prevent the solidification of the alloy before the mold was completely filled. The melt was then poured into the mold. The casting process is illustrated in Fig. 1.

Table 1 Compositions of four solder alloys (wt.%)

Solder alloy	Bi	Sb	Cu	Ag	Sn
SAC0705	−	−	0.547	0.788	98.665
SAC0705−1Bi−1Sb	1.142	1.097	0.536	0.766	96.459
SAC0705−2Bi−2Sb	2.381	1.888	0.491	0.763	94.447
SAC0705−3Bi−3Sb	3.191	3.166	0.539	0.784	92.320

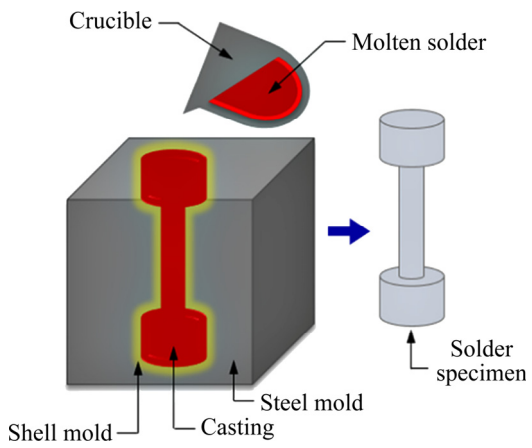

Fig. 1 Schematic diagram of casting process of solder specimens

2.2 Solder specimen characterization

The compositions of the four solder specimens were analyzed by X-ray fluorescence spectrometry (XRF, PANalytical, Zetium). The melting temperature, melting range, and undercooling of solder specimens were determined by differential scanning calorimetry (DSC, NETZSCH, DSC 200F3 Maia), performed in N_2 from 30 to 300 °C at heating and cooling rates of 10 °C/min. Before the observation of microstructures by an optical microscope (OM, Olympus, BX 53) and a scanning

electron microscope (SEM, Quanta 400, FEI), the solder specimens were prepared by the metallographic processes of grinding, polishing, and etching with a solution containing 3 vol.% HCl, 5 vol.% HNO_3, and 92 vol.% CH_3OH for 20 s. The microstructures of solder specimens were analyzed by SEM coupled to an energy dispersive X-ray spectroscope (EDS, Oxford, X-Max^{N}20). The phase identification of solder specimens was confirmed by X-ray diffraction analysis (XRD, PANalytical Empyrean) using Cu K_α radiation (λ(Cu)= 0.15406 nm) in the 2θ range of 10°−120° with a step size of 0.026° and a counting time of 70 s. The sample for XRD analysis was prepared in a disc shape, with the diameter of 12 mm and the thickness of 4 mm. The surface of the sample was polished with SiC sandpaper before testing. The ultimate tensile strength (UTS) and ductility of solder specimens were obtained from tensile testing. The specimens were prepared according to the ASTM E8 standard and tested on a universal testing machine (UTM, Instron 5569) at room temperature and a constant strain rate of 1.5 mm/min. Vickers microhardness testing (model: INNOVATEST, NOVA 130/240) was carried out to determine the hardness values of solder specimens at a load of 200 g and dwell time of 10 s.

3 Results and discussion

3.1 Microstructure of solder alloys

The microstructures of SAC0705, SAC0705−1Bi−1Sb, SAC0705−2Bi−2Sb, and SAC0705−3Bi−3Sb solders were analyzed by OM and SEM. β-Sn phases and eutectic areas can be seen in an OM image of the SAC0705 solder (Fig. 2(a)). The refinement of the β-Sn phase and expansion of the eutectic areas of the SAC0705 alloy after the addition of both Bi and Sb can be seen in images of SAC0705−1Bi−1Sb, SAC0705−2Bi−2Sb, and SAC0705−3Bi−3Sb alloys (Figs. 2(b−d)). The average sizes of β-Sn phases were 7.06, 5.58, 4.23, and 6.30 μm for SAC0705, SAC0705−1Bi−1Sb, SAC0705−2Bi−2Sb, and SAC0705−3Bi−3Sb solders, respectively. The average size of β-Sn phases reduced with the increasing Bi and Sb contents. The addition of Bi and Sb reduced the undercooling of the solders and improved the nucleation of solidified phases, which enhanced heterogeneous nucleation, producing a finer microstructure [21,22,28,37]. Backscatter electron SEM images of the solders revealed microstructures consisting of a β-Sn phase and Cu_6Sn_5 and Ag_3Sn IMC phases in the eutectic areas.

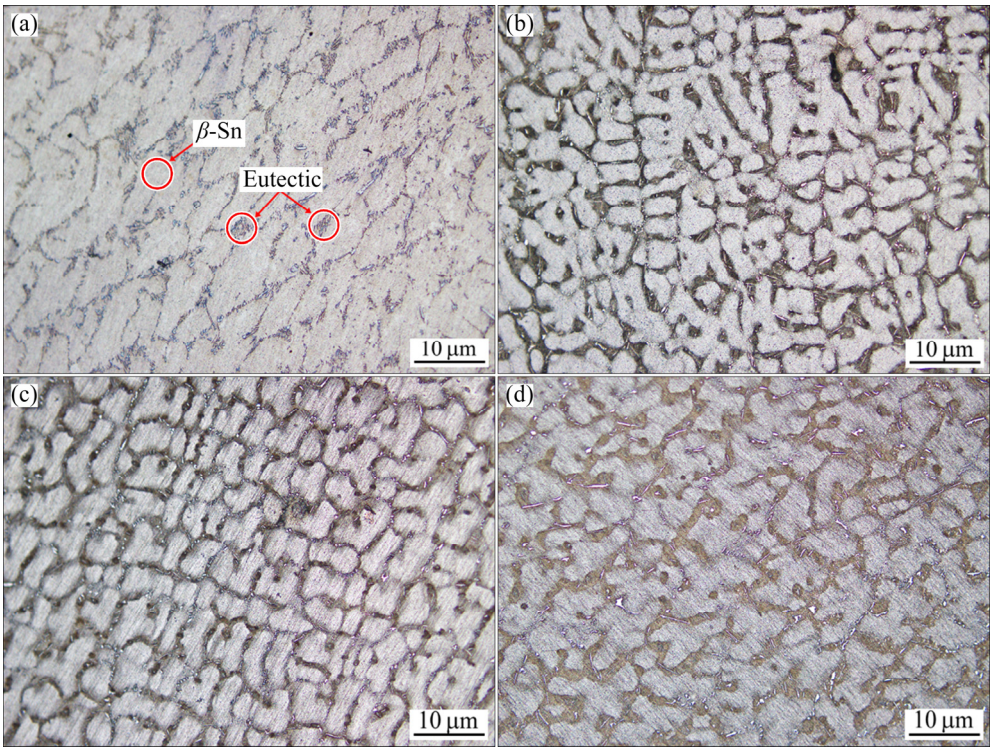

Fig. 2 Microstructures of solder alloys observed by OM: (a) SAC0705; (b) SAC0705−1Bi−1Sb; (c) SAC0705−2Bi−2Sb; (d) SAC0705−3Bi−3Sb

The SAC0705 alloy exhibited rod-like Cu_6Sn_5 phase IMC particles and needle-like Ag_3Sn phase IMC particles (Fig. 3(a)). The addition of Bi and Sb refined the β-Sn matrix and the Cu_6Sn_5 and Ag_3Sn IMC phases by reducing the undercooling of the alloy. The size of the IMC phases decreased (Figs. 3(b−d)). Sb atoms were highly soluble in Sn atoms and formed solid solution phases in the solder matrix [22,27,28] (Fig. 3(d)). On the other hand, the solubility of Bi atoms in Sn atoms was limited and in cases of SAC0705−2Bi−2Sb and SAC0705−3Bi−3Sb, white precipitates of Bi were present in the solder matrix [21,37] (Figs. 3(c, d)). The IMC phases of SAC0705, SbSn phases, and Bi phases of SAC0705−3Bi−3Sb were confirmed by XRD analysis (Fig. 4). The XRD pattern of the SAC0705 solder mainly exhibited strong peaks attributed to β-Sn phase, and small peaks of Ag_3Sn and Cu_6Sn_5 IMC phases (Fig. 4(a)). The small addition of Bi and Sb to SAC0705 solder did not show peaks of Bi and Sb due to forming solid solution phases in the solder matrix (Fig. 4(b)). With increasing Bi and Sb contents, the solubilities of Bi and Sb atoms in Sn atoms were limited, thus precipitates of Bi and SbSn phases in the solder matrix were formed. As a result, small peaks of Bi and SbSn in the SAC0705−3Bi−3Sb solder were observed (Fig. 4(c). The phase compositions of the SAC0705 base solder and SAC0705−3Bi−3Sb solder were analyzed by EDS. The SAC0705 base solder presented only Ag_3Sn and Cu_6Sn_5 IMC phases in the solder matrix, and the composition ratios of the IMCs were 62.0 wt.% Ag : 38.0 wt.% Sn (Point 2), and 36.5 wt.% Cu : 63.5 wt.% Sn (Point 3) as shown in Figs. 5(c, d)), respectively. The SAC0705−3Bi−3Sb solder presented Cu_6Sn_5 and Ag_3Sn IMC phases, with a solid solution phase, and Bi phases in the solder matrix. The composition ratios were 37.2 wt.% Cu : 62.8 wt.% Sn (Point 4), 72.0 wt.% Ag : 28.0 wt.% Sn (Point 5), 92.0 wt.% Sn : 4.0 wt.% Bi : 4.0 wt.% Sb (Point 6), and 67.5 wt.% Bi : 32.5 wt.% Sn (Point 7), as shown in Figs. 6(b−e), respectively. The phase compositions of the solder alloys were summarized in Table 2.

3.2 Thermal properties of solder alloys

The melting temperature is the most important parameter of a solder alloy for use in the electronic

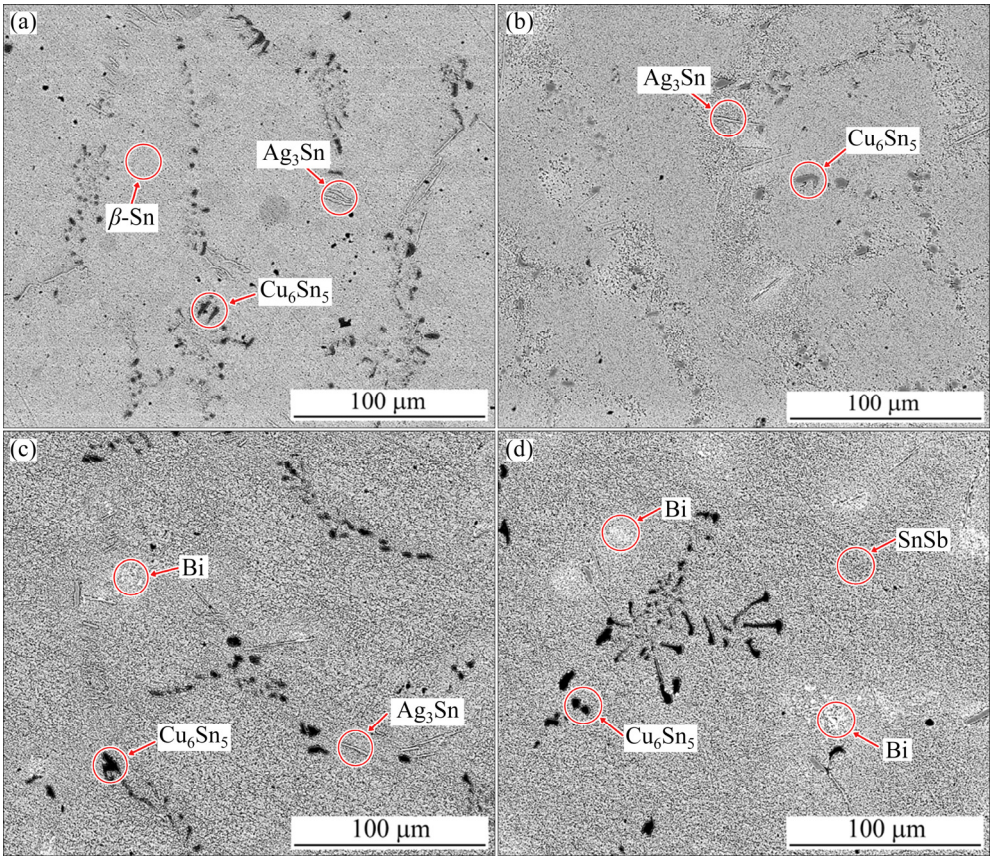

Fig. 3 Microstructures of solder alloys observed by backscatter electron SEM: (a) SAC0705; (b) SAC0705−1Bi−1Sb; (c) SAC0705−2Bi−2Sb; (d) SAC0705−3Bi−3Sb

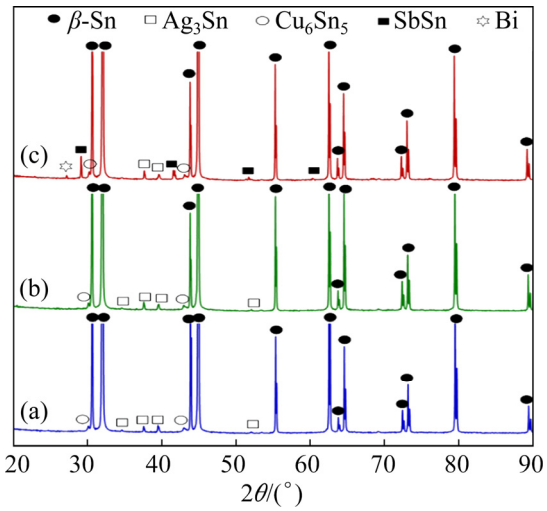

Fig 4 XRD patterns of SAC0705 (a), SAC0705−1Bi−1Sb (b), and SAC0705−3Bi−3Sb (c)

assembly industry. A higher melting temperature will affect the performance of the solder on electronic circuit boards and electronic equipment. The melting temperature, melting range, and undercooling of the SAC0705, SAC0705−1Bi−1Sb, SAC0705−2Bi−2Sb, and SAC0705−3Bi−3Sb solders during heating and cooling processes were analyzed by DSC. The DSC heating curves of all the solder alloys showed two endothermic peaks (Fig. 7). The first peak at the lower temperature indicated the eutectic temperature and the second peak at the higher temperature indicated the melting point of the primary β-Sn phase [26,38]. The melting temperature and melting range of the SAC0705 solder alloy were affected by the addition of Bi and Sb. The melting temperature of the SAC0705−3Bi−3Sb solder was about 4.1 °C higher than that of the SAC0705 solder, while the melting range of the SAC0705−3Bi−3Sb (21.2 °C) was significantly greater than that of the SAC0705 alloy (13.3 °C). The increase was due to the formation of new SbSn phases in the solder matrix [28]. Generally, solder alloys should have a small melting range, not exceeding 30 °C as recommended by LI et al [28]. The melting temperature and melting range values of the present solder alloys are summarized in Table 3. The solidification behavior of a solder alloy is determined by the degree of undercooling, which also affects the microstructure obtained after the solidification process has been

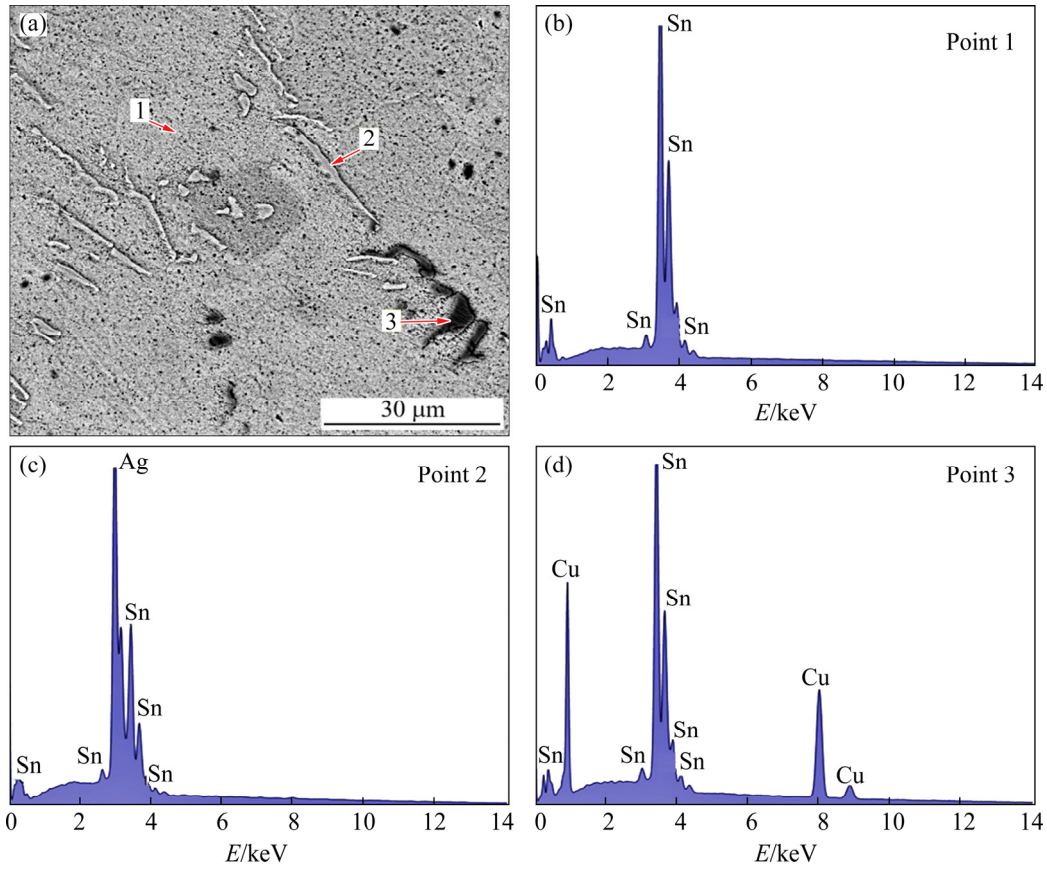

Fig. 5 EDS analysis results of SAC0705 solder alloy: (a) Eutectic area; (b) β-Sn phase; (c) Ag_3Sn IMC; (d) Cu_6Sn_5 IMC

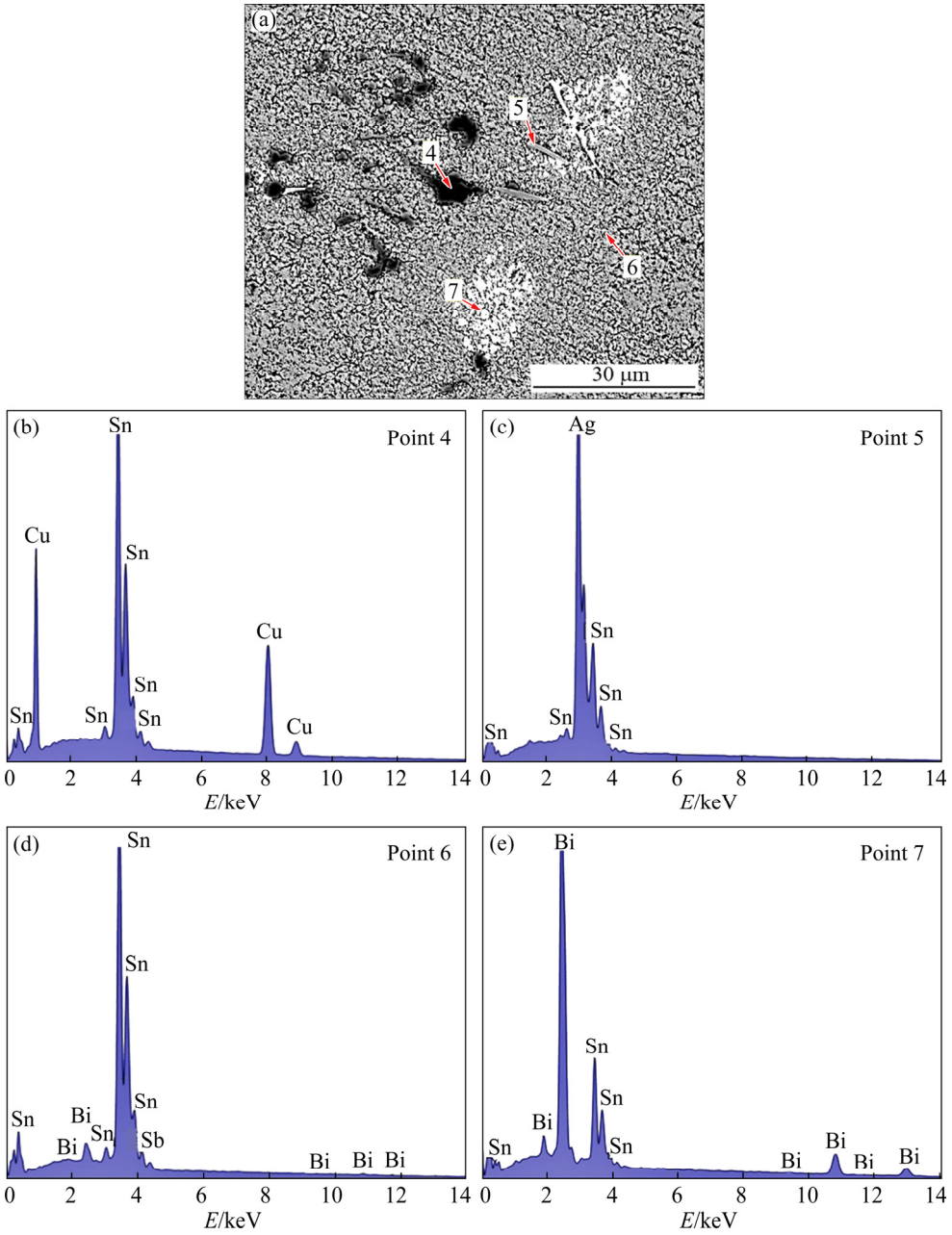

Fig. 6 EDS analysis results of SAC0705−3Bi−3Sb solder alloy: (a) Eutectic area; (b) Cu_6Sn_5 IMC; (c) Ag_3Sn IMC; (d) Solid solution phase; (e) Bi phase

Table 2 EDS analysis results of phase compositions of SAC0705 (Points 1−3 in Fig. 5) and SAC0705−3Bi−3Sb (Points 4−7 in Fig. 6) solder alloys (wt.%)

Point No.	Sn	Ag	Cu	Bi	Sb
1	100	–	–	–	–
2	38.0	62.0	–	–	–
3	63.5	–	36.5	–	–
4	62.8	–	37.2	–	–
5	28.0	72.0	–	–	–
6	92.0	–	–	4.0	4.0
7	32.5	–	–	67.5	–

completed. The undercooling of solder alloys can be calculated from onset heating temperature $T_{onset,1}$ minus onset cooling temperature $T_{onset,2}$. In the studied solder alloys, the addition of Bi and Sb significantly reduced the degree of undercooling of the solders. The undercooling of the SAC0705 alloy was 27.0 °C and that of SAC0705−3Bi−3Sb was 18.9 °C (Table 4). The lower level of undercooling in the Bi- and Sb-added alloys promoted the nucleation of the solidified phase, which multiplied heterogeneous nucleation sites and refined the microstructure [21,26].

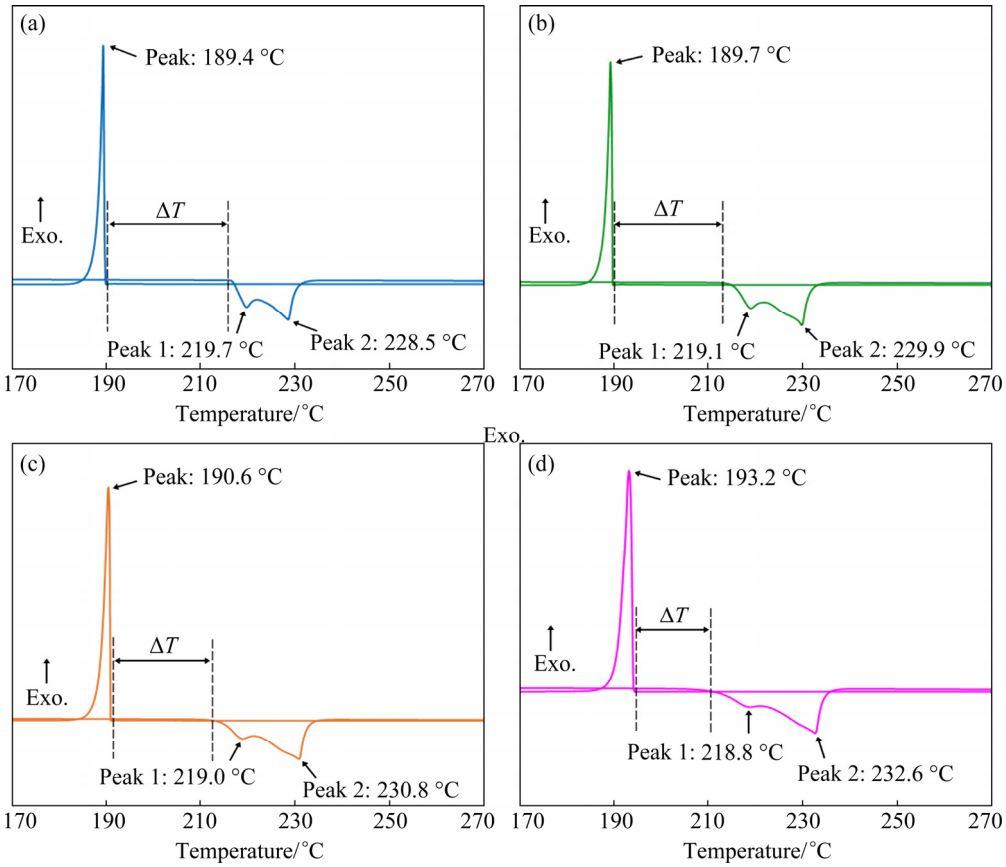

Fig. 7 DSC curves of solder alloys during heating and cooling: (a) SAC0705; (b) SAC0705−1Bi−1Sb; (c) SAC0705−2Bi−2Sb; (d) SAC0705−3Bi−3Sb

Table 3 Data from heating curves showing melting temperature (T_m), solidus temperature (T_{onset}), liquidus temperature (T_{end}), and melting range ($T_{end}-T_{onset}$) of solder alloys

Solder alloy	T_{m_1}/°C	T_{m_2}/°C	T_{onset}/°C	T_{end}/°C	($T_{end}-T_{onset}$)/°C
SAC0705	219.7	228.5	216.7	230.0	13.3
SAC0705−1Bi−1Sb	219.1	229.9	215.4	231.4	16.0
SAC0705−2Bi−2Sb	219.0	230.8	214.6	232.3	17.7
SAC0705−3Bi−3Sb	218.8	232.6	213.0	234.2	21.2

Table 4 Undercooling ($T_{onset,1}-T_{onset,2}$) of solder alloys calculated from heating and cooling curves

Solder alloy	$T_{onset,1}$/°C	$T_{onset,2}$/°C	($T_{onset,1}-T_{onset,2}$)/°C
SAC0705	216.7	189.7	27.0
SAC0705−1Bi−1Sb	215.4	190.2	25.2
SAC0705−2Bi−2Sb	214.6	191.0	23.6
SAC0705−3Bi−3Sb	213.0	194.1	18.9

3.3 Mechanical properties of solder alloys

The combined effect of Bi and Sb was investigated on UTS, elongation (EL), and hardness of the solder alloys. The stress−strain curves of the SAC0705, SAC0705−1Bi−1Sb, SAC0705−2Bi−2Sb, and SAC0705−3Bi−3Sb solder specimens exhibited elastic deformation, plastic deformation, and breaking points. Three samples were measured and labeled as Samples 1, 2, and 3, respectively (Figs. 8(a−d)). The addition of Bi and Sb increased the UTS of the SAC0705 solder from 31.26 to 63.15 MPa in the case of the SAC0705−3Bi−3Sb solder. Meanwhile the EL decreased from 27.93% for the SAC0705 solder to 17.76% for the SAC0705−3Bi−3Sb solder (Fig. 8(e)). The addition of Bi and Sb resulted in finer microstructures, the formation of solid solutions and Bi precipitates in the solder matrix. These modifications combined strengthening mechanisms such as grain boundary

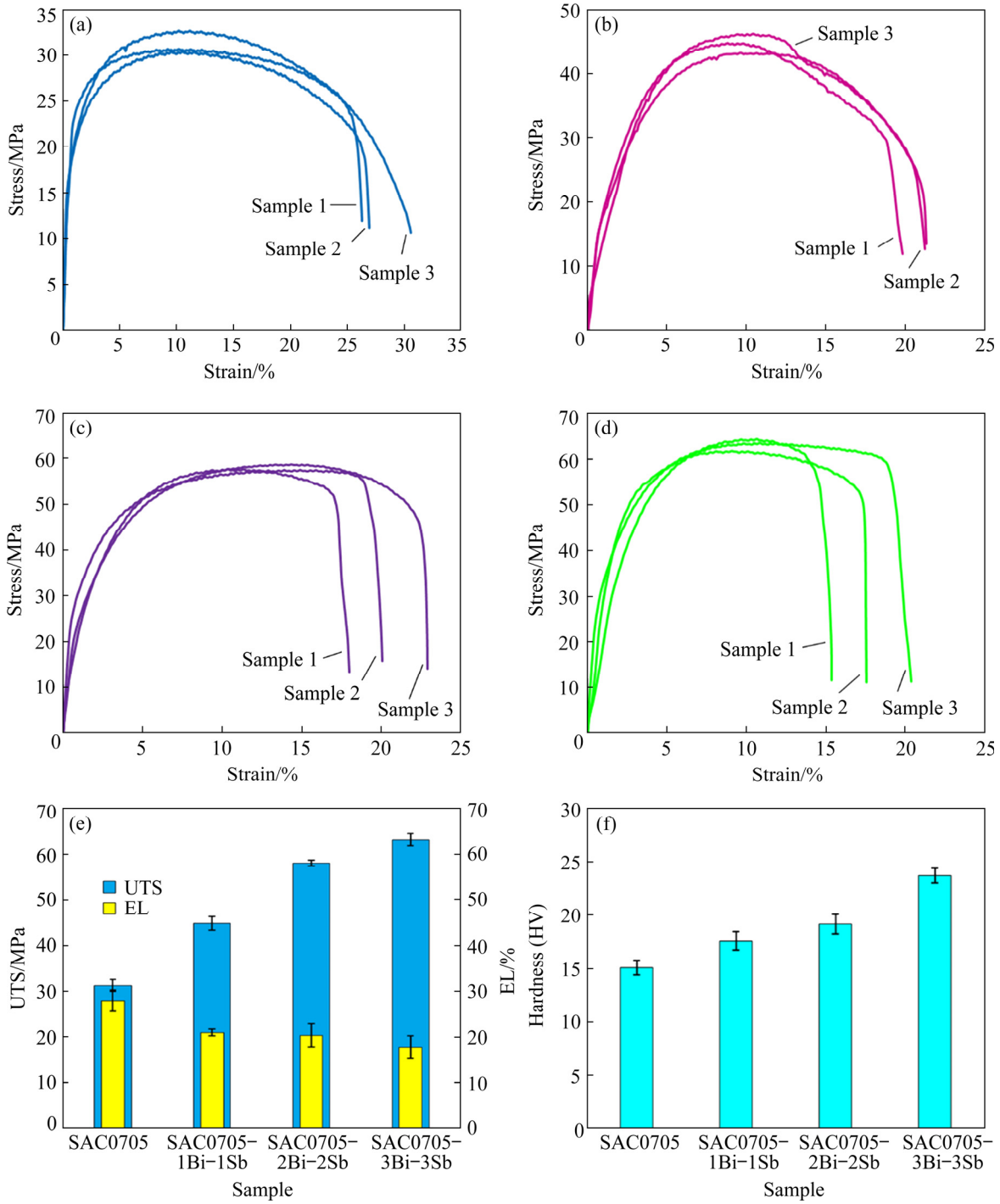

Fig. 8 Stress−strain curves, UTS, EL and hardness of solder alloys from tensile testing: (a) SAC0705; (b) SAC0705−1Bi−1Sb; (c) SAC0705−2Bi−2Sb; (d) SAC0705−3Bi−3Sb; (e) UTS and EL; (f) Hardness

strengthening, solid solution strengthening, and precipitation strengthening that hindered dislocation movement within the crystal structure. Previous research into SAC solder groups added with Bi and Sb found that the effects of grain size reduction strengthening, dispersion precipitates strengthening, and solid solution strengthening increased hardness, yield strength (YS) and UTS, and decreased EL [21,22,25,28,39]. The hardness value of the SAC0705 solder was 15.07 HV, which increased to 23.68 HV for the SAC0705−3Bi−3Sb solder (Fig. 8(f)). This increase was due to the formation of a solid solution and Bi precipitation in the solder matrix [21,28]. The average values of UTS, EL, and hardness of the studied solder alloys are summarized in Table 5. The fracture surfaces of

solder specimens were observed after tensile testing to understand the fracture behavior of the alloys. The fracture surface of the SAC0705 solder showed micro-voids and dimples, which indicated the ductile fracture mode (Fig. 9(a)). The fracture surfaces of the SAC0705−1Bi−1Sb and SAC0705−2Bi−2Sb solders showed fewer dimples and micro-voids, and the fracture surface of the SAC0705−3Bi−3Sb solder showed an obvious cleavage fracture. These morphological changes indicated a gradual transformation from the ductile fracture mode to the brittle fracture mode due to the increasing formation of brittle SbSn phases and Bi phases in the solder matrix [21,28] (Figs. 9(b−d)). The morphological characteristics of the fracture surfaces were consistent with the stress−strain behaviors of the solder alloys represented in the stress−strain curves produced during tensile testing (Fig. 8).

Table 5 Average values of UTS, EL, and hardness of solder alloys

Solder alloy	UTS/MPa	EL/%	Hardness (HV)
SAC0705	31.26	27.93	15.07
SAC0705−1Bi−1Sb	44.74	20.92	17.60
SAC0705−2Bi−2Sb	58.09	20.32	19.11
SAC0705−3Bi−3Sb	63.15	17.76	23.68

4 Conclusions

(1) The microstructure of SAC0705 solder was refined by the addition of Bi and Sb. The grain size of β-Sn phases decreased and the eutectic areas were extended. In addition, the formation of solid solutions phases and Bi phases in the solder matrix affected the mechanical properties of the solder.

(2) The ultimate tensile strength and hardness of the SAC0705-based solders were increased by grain boundary strengthening, solid solution strengthening, and precipitation strengthening. In addition, the fracture mechanism changed from the ductile fracture mode to brittle fracture mode when Bi and Sb were both added to the alloy at 3 wt.%.

(3) The addition of both Bi and Sb to the SAC0705 solder alloy significantly reduced the degree of undercooling, while the melting range and melting temperature of the solders increased.

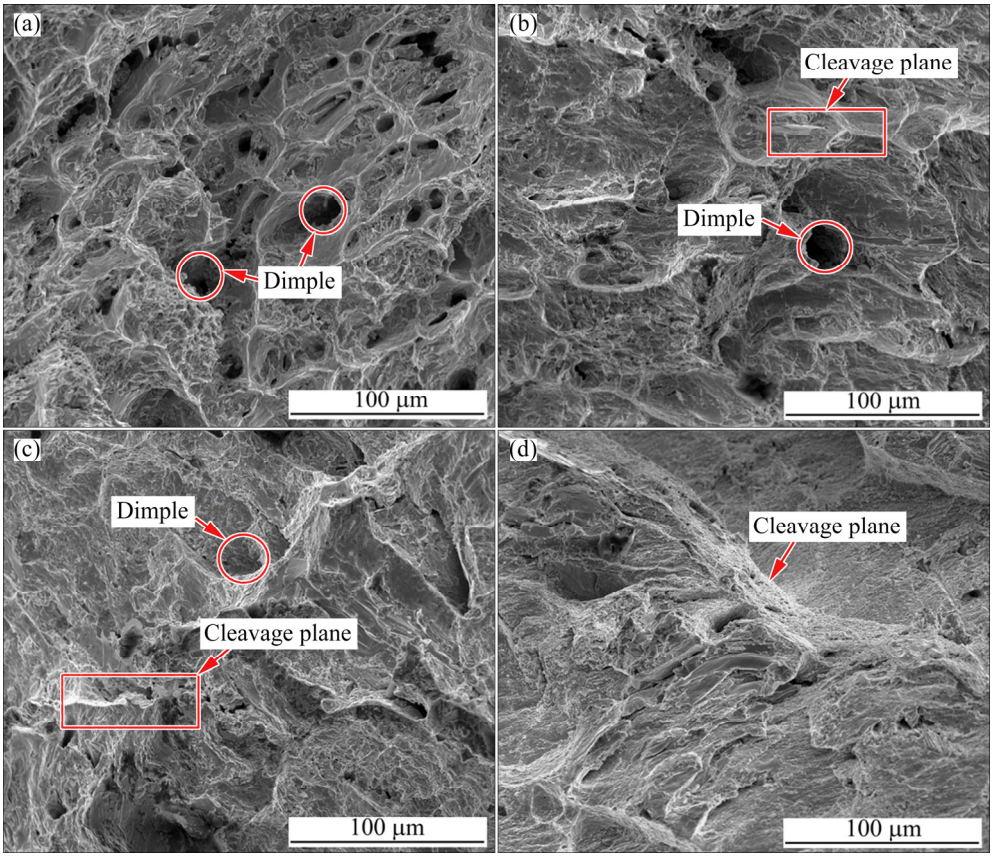

Fig. 9 Fracture surface morphologies of solder alloys: (a) SAC0705; (b) SAC0705−1Bi−1Sb; (c) SAC0705−2Bi−2Sb; (d) SAC0705−3Bi−3Sb

Acknowledgments

This research was supported by the Division of Physical Science, Faculty of Science, Prince of Songkla University (PSU), Thailand. The authors wish to thank academician Thomas Duncan Coyne for improving the English in this paper.

References

[1] EL-DALY A A, HAMMAD A E. Development of high strength Sn−0.7Cu solders with the addition of small amount of Ag and In [J]. Journal of Alloys and Compounds, 2011, 509: 8854−8860.

[2] SOARES T, CRUZ C, SILVA B, BRITO C, GARCIA A, SPINELLI J E, CHEUNG N. Interplay of wettability, interfacial reaction and interfacial thermal conductance in Sn−0.7Cu solder alloy/substrate couples [J]. Journal of Electronic Materials, 2020, 49: 173−187.

[3] TIAN Shuang, LI Sai-peng, ZHOU Jian, XUE Feng. Thermodynamic characteristics, microstructure and mechanical properties of Sn−0.7Cu−*x*In lead-free solder alloy [J]. Journal of Alloys and Compounds, 2018, 742: 835−843.

[4] OSÓRIO W R, LEIVA D R, PEIXOTO L C, GARCIA L R, GARCIA A. Mechanical properties of Sn−Ag lead-free solder alloys based on the dendritic array and Ag_3Sn morphology [J]. Journal of Alloys and Compounds, 2013, 562: 194−204.

[5] ZHANG Liang, HE Cheng-wen, GUO Yong-huan, HAN Ji-guang, ZHANG Yong-wei, WANG Xu-yan. Development of SnAg-based lead free solders in electronics packaging [J]. Microelectronics Reliability, 2012, 52: 559−578.

[6] SILVA B L, XAVIER M G C, GARCIA A, SPINELLI J E. Cu and Ag additions affecting the solidification microstructure and tensile properties of Sn−Bi lead-free solder alloys [J]. Materials Science and Engineering A, 2017, 705: 325−334.

[7] WANG Feng-jiang, CHEN Hong, HUANG Ying, LIU Lu-ting, ZHANG Zhi-jie. Recent progress on the development of Sn−Bi based low-temperature Pb-free solders [J]. Journal of Materials Science: Materials in Electronics, 2019, 30: 3222−3243.

[8] HIRATA Y, YANG C H, LIN S K, NISHIKAWA H. Improvements in mechanical properties of Sn−Bi alloys with addition of Zn and In [J]. Materials Science and Engineering A, 2021, 813: 141131.

[9] DIAS M, COSTA T A, SILVA B L, SPINELLI J E, CHEUNG N, GARCIA A. A comparative analysis of microstructural features, tensile properties and wettability of hypoperitectic and peritectic Sn−Sb solder alloys [J]. Microelectronics Reliability, 2018, 81: 150−158.

[10] SCHON A F, REYES R V, SPINELLI J E, GARCIA A, SILVA B L. Assessing microstructure and mechanical behavior changes in a Sn−Sb solder alloy induced by cooling rate [J]. Journal of Alloys and Compounds, 2019, 809: 151780.

[11] RAMOS L S, REYES R V, GOMES L F, GARCIA A, SPINELLI J E, SILVA B L. The role of eutectic colonies in the tensile properties of a Sn−Zn eutectic solder alloy [J]. Materials Science and Engineering A, 2020, 776: 138959.

[12] WEI Yu-hang, LIU Ying-xia, ZHAO Xiu-chen, TAN Cheng-wen, DONG Ya-ru, ZHANG Ji. Effects of minor alloying with Ge and In on the interfacial microstructure between Zn−Sn solder alloy and Cu substrate [J]. Journal of Alloys and Compounds, 2020, 831: 154812.

[13] WANG Hao-zhong, HU Xiao-wu, JIANG Xion-gxin, LI Yu-long. Interfacial reaction and shear strength of ultrasonically-assisted Sn−Ag−Cu solder joint using composite flux [J]. Journal of Manufacturing Processes, 2021, 62: 291−301.

[14] HO C E, YANG S P, LEE P T, LEE C Y, CHEN C C, KUO T T. IMC microstructure modification and mechanical reinforcement of Sn−Ag−Cu/Cu microelectronic joints through an advanced surface finish technique [J]. Journal of Materials Research and Technology, 2021, 11: 1895−1910.

[15] SUGANUMA K. Advances in lead-free electronics soldering [J]. Current Opinion in Solid State and Materials Science, 2001, 5: 55−64.

[16] CHEN G, WU F S, LIU C Q, SILBERSCHMIDT V V, CHAN Y H. Microstructures and properties of new Sn−Ag−Cu lead-free solder reinforced with Ni-coated graphene nanosheets [J]. Journal of Alloys and Compounds, 2016, 656: 500−509.

[17] LU Tao, YI Dan-qing, WANG Hong-xuan, TU Xiao-xuan, WANG Bin. Microstructure, mechanical properties, and interfacial reaction with Cu substrate of Zr-modified SAC305 solder alloy [J]. Journal of Alloys and Compounds, 2019, 781: 633−643.

[18] KANG S K, SHIH D Y, DONALD N, HENDERSON W, GOSSELIN T, SARKHEL A, CHARLES GOLDSMITH N, PUTTLITZ K J, CHOI W K. Ag_3Sn plate formation in the solidification of near-ternary eutectic Sn−Ag−Cu [J]. JOM, 2003, 55: 61−65.

[19] FALLAHI H, NURULAKMAL M S, AREZODAR A F, ABDULLAH J. Effect of iron and indium on IMC formation and mechanical properties of lead-free solder [J]. Materials Science and Engineering A, 2012, 553: 22−31.

[20] ZHANG Qing-ke, LONG Wei-ming, YU Xin-quan, PEI Yin-yin, QIAO Pei-xin. Effects of Ga addition on microstructure and properties of Sn−Ag−Cu/Cu solder joints [J]. Journal of Alloys and Compounds, 2015, 622: 973−978.

[21] SAYYADI R, NAFFAKH-MOOSAVY H. Physical and mechanical properties of synthesized low Ag/lead-free Sn−Ag−Cu−*x*Bi (*x*=0, 1, 2.5, 5 wt.%) solders [J]. Materials Science and Engineering A, 2018, 735: 367−377.

[22] CHANTARAMANEE S, SUNGKHAPHAITOON P. Influence of bismuth on microstructure, thermal properties, mechanical performance, and interfacial behavior of SAC305−*x*Bi/Cu solder joints [J]. Transactions of Nonferrous Metals Society of China, 2021, 31: 1397−1410.

[23] EL-DALY A A, EL-TAHER A M, GOUDA S. Novel Bi-containing Sn−1.5Ag−0.7Cu lead-free solder alloy with further enhanced thermal property and strength for mobile products [J]. Materials & Design, 2015, 65: 796−805.

[24] ZHAO Jie, QI Lin, WANG Xiu-min, WANG Lai. Influence

of Bi on microstructures evolution and mechanical properties in Sn−Ag−Cu lead-free solder [J]. Journal of Alloys and Compounds, 2004, 375: 196−201.

[25] HAMMAD A E. Enhancing the ductility and mechanical behavior of Sn−1.0Ag−0.5Cu lead-free solder by adding trace amount of elements Ni and Sb [J]. Microelectronics Reliability, 2018, 87: 133−141.

[26] EL-DALY A A, HAMMAD A E, FAWZY A, NASRALLH D A. Microstructure, mechanical properties, and deformation behavior of Sn−1.0Ag−0.5Cu solder after Ni and Sb additions [J]. Materials & Design, 2013, 43: 40−49.

[27] GIURANNO D, DELSANTE S, BORZONE G, NOVAKOVIC R. Effects of Sb addition on the properties of Sn−Ag−Cu/(Cu,Ni) solder systems [J]. Journal of Alloys and Compounds, 2016, 689: 918−930.

[28] LI Chao-jun, YAN Yan-fu, GAO Ting-ting, XU Guo-dong. The microstructure, thermal, and mechanical properties of Sn−3.0Ag−0.5Cu−*x*Sb high-temperature lead-free solder [J]. Materials, 2020, 13: 4443.

[29] EL-DALY A A, EL-HOSAINY H, ELMOSALAMI T A, DESOKY W M. Microstructural modifications and properties of low-Ag-content Sn−Ag−Cu solder joints induced by Zn alloying [J]. Journal of Alloys and Compounds, 2015, 653: 402−410.

[30] HAMMAD A E, RAGAB M. Achieving microstructure refinement and superior mechanical performance of Sn−2.0Ag−0.5Cu−2.0Zn (SACZ) solder alloy with rotary magnetic field [J]. Microelectronics Reliability, 2020, 113: 113932.

[31] CHUANG C L, TSAO L C, LIN H K, FENG L P. Effects of small amount of active Ti element additions on microstructure and property of $Sn_{3.5}Ag_{0.5}Cu$ solder [J]. Materials Science and Engineering A, 2012, 558: 478−484.

[32] SABRI M F M, SHNAWAH D A, BADRUDDIN I A, SAID S B M, CHE F X, ARIGA T. Microstructural stability of Sn−1Ag−0.5Cu−*x*Al (*x*=1, 1.5, and 2 wt.%) solder alloys and the effects of high-temperature aging on their mechanical properties [J]. Materials Characterization, 2013, 78: 129−143.

[33] KANTARCIOĞLU A, KALAY Y E. Effects of Al and Fe additions on microstructure and mechanical properties of SnAgCu eutectic lead-free solders [J]. Materials Science and Engineering A, 2014, 593: 79−84.

[34] MA Z H, BELYAKOV S A, GOURLAY C M. Effects of cobalt on the nucleation and grain refinement of Sn−3Ag−0.5Cu solders [J]. Journal of Alloys and Compounds, 2016, 682: 326−337.

[35] WU Jie, XUE Song-bai, WANG Jing-wen, WU Ming-fang. Coupling effects of rare-earth Pr and Al_2O_3 nanoparticles on the microstructure and properties of Sn−0.3Ag−0.7Cu low-Ag solder [J]. Journal of Alloys and Compounds, 2019, 784: 471−487.

[36] ZHANG Liang, FAN Xi-ying, GUO Yong-huan, HE Cheng-wen. Properties enhancement of SnAgCu solders containing rare earth Yb [J]. Materials & Design, 2014, 57: 646−651.

[37] SAYYADI R, NAFFAKH-MOOSAVY H. The role of intermetallic compounds in controlling the microstructural, physical and mechanical properties of Cu−[Sn−Ag−Cu−Bi]−Cu solder joints [J]. Scientific Reports, 2019, 9: 1−20.

[38] HAMMAD A E. Evolution of microstructure, thermal and creep properties of Ni-doped Sn−0.5Ag−0.7Cu low-Ag solder alloys for electronic applications [J]. Materials & Design, 2013, 52: 663−670.

[39] LI G Y, CHEN B L, SHI X Q, WONG S C K, WANG Z F. Effects of Sb addition on tensile strength of Sn−3.5Ag−0.7Cu solder alloy and joint [J]. Thin Solid Films, 2006, 504: 421−425.

Bi 和 Sb 元素对 Sn−0.7Ag−0.5Cu 焊料合金显微组织、热性能和力学性能的影响

Suchart CHANTARAMANEE[1], Phairote SUNGKHAPHAITOON[2]

1. Department of Industrial Engineering, Faculty of Engineering,
Rajamangala Unversity of Technology Srivijaya, 90000 Songkhla, Thailand;
2. Division of Physical Science, Faculty of Science, Prince of Songkla University, Hat Yai, 90110 Songkhla, Thailand

摘　要：研究添加 Bi 和 Sb 元素对 Sn−0.7Ag−0.5CU(SAC0705)焊料合金显微组织、热性能、极限抗拉强度、延展性和硬度的共同影响。结果表明，Bi 和 Sb 的加入显著降低焊料的过冷度，细化焊料的 β-Sn 相以及扩大焊料的共晶区域。此外，焊料基体中 SbSn 相和 Bi 相的形成也影响焊料的力学性能。添加 3%(质量分数)的 Bi 和 3%(质量分数)的 Sb 后，SAC0705 合金的极限抗拉强度和硬度从 31.26 MPa 和 15.07 HV 分别提高到 63.15 MPa 和 23.68 HV。焊料合金的晶界强化、固溶强化和析出强化以及断裂机制的改变导致其延展性降低。

关键词：Sn−0.7Ag−0.5Cu 焊料合金；金属间化合物；强化机制；过冷度；力学性能

(Edited by Wei-ping CHEN)